HHS Public Access

Author manuscript

Nature. Author manuscript; available in PMC 2016 August 03.

Published in final edited form as:

Nature. 2016 February 11; 530(7589): 184–189. doi:10.1038/nature16932.

Naturally occurring p16^{Ink4a}-positive cells shorten healthy lifespan

Darren J. Baker[1], **Bennett G. Childs**[2], **Matej Durik**[1], **Melinde E. Wijers**[1], **Cynthia J. Sieben**[2], **Jian Zhong**[1], **Rachel Saltness**[1], **Karthik B. Jeganathan**[1], **Grace C. Versoza**[3], **Abdul-Mohammad Pezeshki**[4], **Khashayarsha Khazaie**[4], **Jordan D. Miller**[3], and **Jan M. van Deursen**[1,2]

[1]Department of Pediatric and Adolescent Medicine, Mayo Clinic College of Medicine, Rochester, Minnesota 55905, USA

[2]Department of Biochemistry and Molecular Biology, Mayo Clinic College of Medicine, Rochester, Minnesota 55905, USA

[3]Division of Cardiovascular Surgery, Mayo Clinic College of Medicine, Rochester, Minnesota 55905, USA

[4]Department of Immunology, Mayo Clinic College of Medicine, Rochester, Minnesota 55905, USA

Abstract

Cellular senescence, a stress-induced irreversible growth arrest often characterized by p16^{Ink4a} expression and a distinctive secretory phenotype, prevents the proliferation of preneoplastic cells and has beneficial roles in tissue remodelling during embryogenesis and wound healing. Senescent cells accumulate in various tissues and organs over time and have been speculated to play a role in aging. To explore the physiological relevance and consequences of naturally occurring senescent cells, we used a previously established transgene, *INK-ATTAC*, to induce apoptosis in p16^{Ink4a}-expressing cells of wild-type mice by injection of AP20187 twice a week starting at one year of age. Here we show that compared to vehicle alone, AP20187 treatment extended median lifespan in both male and female mice of two distinct genetic backgrounds. Clearance of p16^{Ink4a}-positive cells delayed tumorigenesis and attenuated age-related deterioration of several organs without apparent side effects, including kidney, heart and fat, where clearance preserved the functionality

Correspondence and requests for materials should be addressed to J.M.v.D. (; Email: vandeursen.jan@mayo.edu) or D.J.B. (; Email: baker.darren@mayo.edu)

Author contributions

D.J.B. performed all lifespan and most healthspan analyses on *ATTAC* mice. B.G.C. designed and conducted experiments to identify and quantitate X-GAL-positive cells by TEM, and analyzed mice for cardiomyocyte hypertrophy and local RAAS activity in kidney. M.E.W. J.Z. and R.S. assisted with various aspects of healthspan analyses: the extent of their contributions is reflected in the authorship order. C.J.S. conducted the lifespan analysis of C57BL/6-129Sv/E hybrid mice on diets containing 5% or 9% fat. K.B.J. investigated somatotrophic axis signaling. G.C.V., D.J.M. and M.D. analyzed resting heart functions by echocardiography. M.D. designed and conducted cardiac stress tests. A.P. and K.K. analyzed leukocyte subpopulations. J.M.v.D., D.J.B. and B.C. wrote the paper with input from all co-authors. J.M.v.D. directed and supervised all aspects of the study in collaboration with D.J.B.

The authors declare competing financial interests. Details are available in the online version of the paper. J.M.v.D. and D.J.B. are inventors on patents licensed to Unity Biotechnology by Mayo Clinic and J.M.v.D. is a co-founder of Unity Biotechnology. Readers are welcome to comment on the online version of this article at www.nature.com/nature.

of glomeruli, cardio-protective K_{ATP} channels, and adipocytes, respectively. Thus, $p16^{Ink4a}$-positive cells that accumulate during adulthood negatively influence lifespan and promote age-dependent changes in multiple organs, and their therapeutic removal may be an attractive approach to extend healthy lifespan.

Introduction

Cellular senescence is a well-established cancer defense mechanism that has been also hypothesized to play a role in aging and age-associated diseases, presumably through depletion of stem and progenitor cells, and the adverse actions of the senescence-associated secretory phenotype (SASP), which consists of many proinflammatory cytokines and chemokines, matrix metalloproteinases and growth factors[1–3]. Consistent with this idea is the observation that interference with senescent cell accumulation in BubR1 progeroid mice delays several aging-associated disorders that these animals develop[4, 5]. However, because progeroid syndromes do not faithfully mimic the complex degenerative changes of aging, the relevance of these findings has remained unclear. Furthermore, recent studies showing that senescent cells have beneficial effects in injury repair and tissue remodelling[6–10] have called into question the simplistic view of senescence as only a driver of age-dependent pathologies, raising the specter that senescent cell clearance might remove useful cells in addition to detrimental ones. Here we investigated the identity and physiological impact of naturally occurring senescent cells using *INK-ATTAC (*hereafter *AT-TAC)*[4], a transgenic mouse that expresses FKBP-Casp8 and GFP under the control of a minimal $p16^{Ink4a}$ promoter fragment transcriptionally active in senescent cells[4, 11]. Earlier we have shown that, in BubR1 progeroid mice, *ATTAC* ablates $p16^{Ink4a}$-positive senescent cells upon administration of AP20187 (AP), a dimerizer that activates FKBP-fused Casp8[4]. Our first objective was to validate the properties of *ATTAC* in naturally occurring $p16^{Ink4a}$-positive senescent cells.

ATTAC clears senescent adipocyte progenitor cells

Our initial validation was focussed on fat. We collected GFP^+ and GFP^- cell populations from inguinal white adipose tissue (iWAT) of 12-month-old *ATTAC* mice by FACS (Fig. 1a). GFP^+ cells expressed much higher levels of $p16^{Ink4a}$ and *FKBP-Casp8* than GFP^- cells, as well as a broad panel of senescence markers (Fig. 1b). GFP^+ cells, but not GFP^- cells, were also highly positive for senescence-associated-β-galactosidase (SA-β-Gal; Fig. 1c). Furthermore, intact iWAT from aged, but not young *ATTAC* mice had SA-β-Gal activity, but less than iWAT of BubR1 progeroid mice, a difference also reflected in $p16^{Ink4a}$, *FKBP-Casp8*, and *GFP* transcript levels (Extended Data Fig. 1a, b).

iWAT of 18-month-old *ATTAC* mice treated bi-weekly with AP from 12 months on had 8-fold less GFP^+ adipocyte progenitors than vehicle-injected controls, although total progenitor cell numbers remained unchanged (Fig. 1d and Extended Data Fig. 1c). SA-β-Gal staining and qRT-PCR analysis of senescence markers confirmed that $p16^{Ink4a}$-positive senescent cells in iWAT increased between 12 and 18 months and that AP eliminated most of these cells (Fig. 1e and Extended Data Fig. 1d). Consistent with senescence of progenitor

cells, transmission electron microscopy (TEM) on SA-β-Gal-stained iWAT showed that X-Gal crystals were present in small perivascular cells rather than endothelium, white blood cells or adipocytes (Fig. 1f). X-Gal crystals were found in 0.2% and 1.6% of total iWAT cells from AP-treated and control mice, respectively (Fig. 1g).

Clearance of *p16*^{Ink4a}-positive cells prevented loss of fat mass occurring between 12 and 18 months (Fig. 1h, i and Extended Data Fig. 1e). Age-dependent fat tissue dysfunction is characterized by decreased adipogenesis and adipocyte atrophy[12]. Consistent with this, adipocyte size decreased between 12 and 18 months of age (Fig. 1j), as did transcript levels of two key transcriptional regulators of adipogenesis, PPARγ and C/EBPα (Fig. 1k). AP treatment of *ATTAC* mice prevented these decreases. Collectively, these data indicate that senescence contributes to age-dependent fat tissue alterations.

Adipose tissue of young *ATTAC* mice lacked SA-β-Gal activity but contained p16^{Ink4a} (Extended Data Fig. 1a, f–h). This p16^{Ink4a} pool did not decline upon AP treatment. Similar results were obtained with early passage *ATTAC* MEFs (Extended Data Fig. 1i–k), indicating that baseline *p16*^{Ink4a} promoter activity in non-senescent cells is insufficient for FKBP-Casp8-mediated apoptosis. Furthermore, *ATTAC* lacks *p16*^{Ink4a} promoter elements required for transgene induction in replicating pre-neoplastic cells that robustly express endogenous *p16*^{Ink4a} due to Rb inactivation and AP fails to kill these cells (Extended Data Fig. 2a–g). *ATTAC* was also not induced in peripheral blood T lymphocytes that robustly engage endogenous *p16*^{Ink4a} with aging without concomitant expression of multiple senescence markers[2, 13] (Extended Data Fig. 2h), further implying that transgene induction is quite selective for senescence. However, these limited analyses certainly do not exclude the possibility that other *p16*^{Ink4a}-positive non-senescent cells engage *ATTAC* and die upon AP exposure (Supplementary Text).

Clearance by *ATTAC* is partial and tissue selective

To extend our analysis of the properties of *ATTAC*, we analyzed the transcript levels of *p16*^{Ink4a}, *FKBP-Casp8, GFP*, and a panel of senescence markers in a broad spectrum of tissues of 2-, 12-, and 18-month-old untreated *ATTAC* mice, including skeletal muscle, eye, kidney, lung, heart, liver, colon and spleen. *ATTAC* mice treated with AP between 12 and 18 months were included to assess senescent cell clearance rates. *p16*^{Ink4a} expression markedly increased between 12 and 18 months in all tissues examined, which coincided with the induction of *FKBP-Casp8*, *GFP* and multiple senescence markers (Extended Data Fig. 3a). Elevated expression of these transcripts was blunted to varying degrees by AP treatment in all tissues examined but colon and liver, indicating that the *ATTAC* system eliminates *p16*^{Ink4a}-positive senescent cells in a partial and tissue/organ selective fashion. Blunting of age-dependent increases in *Il6*, *Il1a*, and *TNFα* expression in fat, skeletal muscle and kidney by AP treatment (Extended Data Fig. 3b) suggests that *p16*^{Ink4a}-positive cell clearance ameliorates inflammation in these tissues.

p16^{Ink4a}-positive cells shorten lifespan and healthspan

To examine the impact of *p16*^{Ink4a}-positive cell clearance on health and lifespan, we sequentially established two cohorts of *ATTAC* transgenic mice (Fig. 2a). The initial cohort was on a C57BL/6-129Sv-FVB mixed genetic background fed a diet containing 9% fat. We note that this diet shortens lifespan compared to diets with 5% fat typically used in lifespan studies (Extended Data Fig. 4a, b and Supplementary Text). The later cohort was on a congenic C57BL/6 background fed a standard 5% fat diet. At 12 months of age, when *p16*^{Ink4a}-positive cells started to accumulate in several tissues (Extended Data Figs. 1d and 3a), mice were injected twice a week with AP or vehicle until they became moribund or died of natural causes. Mice separate from the longevity cohorts were examined for a series of age-sensitive outcomes at 18 months, an age where relatively few mice in each of the cohorts had died. Data for both sexes combined showed that median lifespans of mixed and C57BL/6 AP-treated animals were increased by 27% and 24%, respectively. Median lifespans for each sex separately were also significantly extended in AP-treated cohorts irrespective of genetic background, with increases ranging from 17% to 35% (Fig. 2b, c).

Maximum lifespan[14] was significantly increased for mixed AP-treated males and females combined ($p = 0.0295$), but not for females and males individually. Maximum lifespan was not extended for C57BL/6 AP-treated animals, either combined or separately. Importantly, AP treatment of mice lacking the *ATTAC* transgene did not improve lifespan (Fig. 2c). We note that the median lifespan of vehicle-treated C57BL/6 males, but not females, was short of the normal range of lifespans for unmanipulated males of this strain at different laboratories (Extended Data Fig. 4c, d)[15–28], suggesting that repetitive vehicle injection stress may have negatively impacted C57BL/6 male longevity (Supplemenary Text).

In both cohorts, AP treatment had no impact on the incidence or spectrum of macroscopically detectable tumors at autopsy, although tumor latency was increased (Fig. 3a and Extended Data Fig. 5a–d). Median lifespan extensions of AP-treated mice dying without tumors ranged from 24% to 42% (Extended Data Fig. 5e), indicating that increased longevity was not merely due to a tumor-protective effect. AP-treated mice were overtly indistinguishable from vehicle-injected littermates at 18 months of age, but typically had a healthier appearance by 22 months (Fig. 3b). AP treatment delayed cataract formation in both males and females on a C57BL/6 background (Extended Data Fig. 5f, g). Despite a lack of overt difference at 18 months, AP-treatment prevented age-dependent reductions in both spontaneous activity and exploratory behavior measured by open-field testing (Fig. 3c), which was sex and genetic background independent.

Extended tests on these mice showed no differences in motor coordination and balance, memory, exercise ability, and muscle strength (Extended Data Fig. 6), indicating that 6 months of *p16*^{Ink4a}-positive cell clearance did not impact these age-sensitive treats. Similarly, age-related changes in the circulating hematopoietic profile, including regulatory T-cell levels, were also not impacted (Extended Data Fig. 7). At 18 months, fasting glucose levels, glucose tolerance, insulin sensitivity and circulating IGF1 levels were not significantly different in AP- and vehicle-treated C57BL/6 *ATTAC* females, as was

signalling downstream of IGF1 and insulin receptors in fat, kidney, and muscle, three tissues where we observed clearance of *p16*^{Ink4a}-positive cells (Extended Data Fig. 8).

Renal epithial cell senescence and glomerulosclerosis

To further investigate the impact of *p16*^{Ink4a}-positive cells on physiological functions that change with age[29], we focussed on kidney and heart, two vital organs in which we observed *ATTAC*-mediated clearance. Aged kidneys are characterized by the formation of sclerotic glomeruli, which affect glomerular filtration rates, impair kidney function, and lead to elevated blood urea nitrogen (BUN) levels[30, 31]. Indeed, glomerulosclerosis significantly increased between 12 and 18 months in vehicle-treated *ATTAC* mice. AP treatment markedly reduced glomerulosclerosis independent of sex and genetic background (Fig. 4a, b), which correlated with attenuated age-related increases in BUN (Fig. 4c), indicating preserved kidney function. SA-β-Gal staining of kidney sections confirmed that AP-mediated disposal of senescent cells was quite efficient (Fig. 4d). By TEM, we observed X-Gal crystals in 0.3% and 1.2% of renal cells of 18-month-old treated and untreated mice, respectively (Fig. 4e, f). Surprisingly, SA-β-Gal-positive cells were not located in the glomeruli but in proximal tubules (Fig. 4e), raising the question as to how senescent tubular brush-border epithelial cells might promote glomerulosclerosis.

Angiotensin receptor blockers attenuate age-related glomerulosclerosis under normotensive conditions, which has led to the idea that overactivation of the local renin-angiotensin-aldosterone system (RAAS) drives the formation of sclerotic glomeruli[31, 32]. Consistent with this, kidney transcript levels of a key component of this system, angiotensin receptor 1a (Agtr1a), increased between 12 and 18 months (Fig. 4g). In contrast, no such increase was observed in AP-treated mice. Western blotting confirmed that Agtr1a was lower in AP-treated kidney samples (Fig. 4h). Both renal tubules and glomeruli contributed to this decline, as demonstrated by immunolabeling of kidney sections for Agtr1a (Fig. 4i). These data suggest that senescent renal epithelial cells may produce SASP components that hyperactivate the local RAAS in kidney.

p16^{Ink4a}-positive cells contribute to cardiac aging

Hearts of 12-month-old mice showed SA-β-Gal activity at the atrial and ventricular surface (Fig. 5a), which increased with aging in vehicle-treated but not AP-treated mice. TEM revealed that ciliated epithelial cells and fibroblasts in the pericardium contained X-Gal crystals (Fig. 5b, c). We also observed SA-β-Gal-positive smooth muscle cells in the aortic root wall of vehicle-treated animals (Fig. 5a and Extended Data Fig. 9a). At 18 months, vehicle- and AP-treated *ATTAC* mice analyzed by echocardiography showed no significant differences in heart rate, left ventricular mass, thickness and diameter, ejection fraction and fractional shortening, all of which were also unchanged from 12-month-old mice (Extended Data Fig. 9b–g). Cardiac aging at the histological level is characterized by a loss of ventricular cardiomyocytes due to decreasing ability to replace apoptotic or necrotic cardiomyocytes, inducing hypertrophy of the remaining cardiomyocytes[33]. Morphometric analysis of heart sections showed that ventricular wall thickness was the same in vehicle- and AP-treated animals, regardless of sex (Fig. 5d). Ventricular cardiomyocytes of AP-

treated mice, however, were much smaller (Fig. 5e, f), implying that they had more cardiomyocytes than vehicle-treated mice. Taken together, these data suggest that *p16*^{Ink4a}-positive cells are key drivers of this age-related cardiac phenotype.

Cardiac aging is also characterized by decreasing stress tolerance, which has been attributed to decreasing numbers of ATP-sensitive potassium (K_{ATP}) channels in the sarcolemma of cardiac myocytes due to age-related reduction in expression of Sur2a, a key regulatory subunit of K_{ATP} channels[34]. Cardiac *Sur2a* expression indeed decreased between 12 and 18 months in vehicle-treated mice (Fig. 5g), but no such decline was observed in AP-treated mice, suggesting that cardiac stress tolerance was preserved. To test this, we measured the time to death from arrhythmogenesis after injection of 580 mg.kg^{-1} of the β-adrenergic agonist isoproterenol[35]. Consistent with age-related loss of cardiac stress resistance, 18-month-old vehicle-treated mice died faster than 12-month-old mice (Fig. 5h). In contrast, time to death was not accelerated in AP-treated mice. In a second, more physiological stress test, we conducted echocardiographic measurements of ventricular mass before and after eliciting cardiac stress over a 6-day period by administering 10 mg.kg^{-1} isoproterenol twice a day. Cardiac mass significantly increased in 18-month-old vehicle-treated mice, whereas AP-treated mice were capable of handling the applied stress without such adaptive response, similar to young mice (Fig. 5i).

We also examined whether AP-treatment caused any off-target or detrimental effects. Wild-type mice lacking *ATTAC* did not show healthspan improvements when treated with AP (Extended Data Fig. 9h–l). Consistent with a beneficial role of senescent cells only for the duration of wound repair[6–8], 18-month-old AP-treated *ATTAC* mice repaired cutaneous wounds when drug administration was suspended during healing (Extended Data Fig. 10a–c). When AP was administered during wound closure, healing was delayed with similar kinetics as 4- or 18-month-old *ATTAC* mice without prior AP treatment, indicating that acute senescence mechanisms are preserved with aging and not influenced by constitutive clearance of senescent cells[3]. Furthermore, 18-month-old AP-treated mice showed no evidence of increased fibrosis in skin and other tissues, despite a role for senescent cells in limiting fibrosis during tissue repair (Extended Data Fig. 10d).

Discussion

Here we eliminated *p16*^{Ink4a}-positive cells from non-progeroid mice using *ATTAC* to begin to address how senescent cells impact health and lifespan. We observe median lifespan extensions in AP-treated *ATTAC* mice on two distinct genetic backgrounds and diets, indicating that age-related accumulation of *p16*^{Ink4a}-positive cells negatively impacts longevity. It will be useful to further optimize senescent cell removal protocols and methods because the longevity of male C57BL/6 mice seemed negatively impacted by repetitive vehicle injection stress, and because clearance was partial and several key tissues were refractory to clearance, including liver and colon. This would be particularly relevant for further studies of maximum lifespan, extension of which is thought to be reflective of a more generalizable “anti-aging” effect[29] (Supplementary Text).

These methodological caveats aside, we find that removal of *p16*^{Ink4a}-positive cells from midlife on delays the progression of neoplastic disease irrespective of genetic background and diet. Clearance had no impact on the spectrum or incidence of postmortem tumors, which is consistent with the hypothesis that senescent cells help create a tissue microenvironment that promotes tumor progression[1]. In addition, multiple age-dependent changes[29], including alterations in fat, eye, heart, kidney, as well as the age-dependent decline in spontaneous activity and exploratory behavior, occur more slowly during a six-month period of *p16*^{Ink4a}-positive cell clearance starting at midlife. Complementary mechanistic studies suggest that local *p16*^{Ink4a}-positive cells in fat, kidney, and heart exert their effects through distinct mechanisms, involving progenitor cell dysfunction, RAAS overactivation, and Sur2a downregulation, respectively, although systemic effects cannot be excluded given the global nature of the clearance method applied here.

Thus, our data best fit a model in which *p16*^{Ink4a}-positive cells act to shorten healthy lifespan by promoting tumor progression and age-dependent changes that functionally impair certain tissues and organs, including vital organs such as kidney and heart. This, together with the key observation that elimination of *p16*^{Ink4a}-positive cells is not associated with any overt detrimental effects raise the possibility that this approach may be useful to treat aspects of age-related functional decline, age-related diseases that involve senescent cells, or side-effects of therapies that create senescent cells[36].

METHODS

Mouse strains and drug treatments

All studies described using *ATTAC* mice were performed on transgenic line 3, which contains 13 copies of the transgene inserted into a single locus (data available upon request). The generation and characterization of the *ATTAC* transgenic line has been previously described in detail[4]. Two cohorts of *ATTAC* mice were consecutively established and analyzed. The first cohort consisted of mice on a mixed 129Sv (40% ±5%) × C57BL/6J (35% ±5%) × FVB (20% ±5%) genetic background as determined by Harlan Laboratories using established SNP panels (Supplementary Table 1). These mice were fed an irradiated pelleted breeder chow diet ad libitum for the entire duration of the study: LabDiet product #5058, with 9% fat content (21.635% calories from fat). Mice from this cohort were randomly assigned to be injected with AP20187 (B/B homodimerizer, Clontech, Mountain View, CA, USA) or vehicle twice a week beginning at 12 months of age. Dosing was 0.2 μg AP20817/g body weight between 12 and 18 months (the same dose as previously used for senescent cell clearance in BubR1 progeroid mice; see reference 4), and 2.0 μg AP20187/g body weight from thereon. The second cohort was established ~1.5 years later after completion of *ATTAC* line 3 backcrossing onto a pure C57BL/6J genetic background (Jackson Lab stock number 000664). Detailed breeding information for the C57BL/6 *ATTAC* cohort is provided in Supplementary Table 2. For the entire duration of the study, congenic *ATTAC* transgenic mice were maintained ad libitum on standard irradiated pelleted chow diet: LabDiet product #5053 with 5% fat content (13.205% calories from fat). The number of mice in the C57BL/6J cohort was increased compared to the mixed cohort to allow for more comprehensive healthspan analyses at 18 months of age. The C57BL/6J

cohort was randomly assigned to receive either 2.0 μg AP20187/g body weight or vehicle from 12 months until the end of life. Non-transgenic mice from C57BL/6J *ATTAC* transgenic crosses were used to establish the control cohort for confirmation that AP20187 had no impact on healthspan in the absence of the *ATTAC* transgene. *BubR1*$^{H/H}$*;ATTAC* mice used in this study were generated as previously described[4]. Animals were housed in a pathogen-free barrier environment throughout the duration of the study and kept on a 12-h light-dark cycle. Specifically, mice were housed 5/cage in static autoclaved HEPA-ventilated microisolator cages measuring 446 cm^2 (27 × 16.5 × 15.5 cm), which are opened only within Class II biosafety cabinets. Restricted entry to the room requires key card access to unlock the door. Entrance into the barrier facility requires wearing autoclaved gowns, disposable gloves, caps, and shoe covers. Personnel are not allowed to enter any other rodent facility prior to entry into the barrier. Mouse colonies in this facility are monitored through contact sentinels (one cage per rodent rack) which are evaluated quarterly for (and are free of) the following agents: Sendai virus, pneumonia virus of mice (PVM), mouse hepatitis virus (MHV), minute virus of mice (MVM), Theiler's murine encephalomyelitis virus (TMEV strain GDVII), reovirus, rotavirus (EDIM), mouse parvovirus (MPV strain 1 and 2), murine norovirus (MNV), *Mycoplasma pulmonis*, *Aspiculuris tetraptera* and *Syphacia* spp. In addition, the following are annually screened for (and free of) these agents: lymphocytic choriomeningitis virus (LCMV), ectromelia virus (mousepox), K virus, polyoma virus, mouse adenovirus (MAV type 1 and 2), hantavirus, Prospect Hill virus (PHV), mouse cytomegalovirus (MCMV), lactate dehydrogenase dlevating virus (LDEV) *Encephalitozoon cuniculi*, cilia-associated respiratory bacillus (CARB), mouse thymic virus (MTV, MTLV), *Clostridium piliforme*, *Myobia* spp and *Myocoptes* spp. Autoclaved Enrich-o'Cobs (The Andersons Incorporated, Maumee, OH, USA) were used as bedding. Cages and bedding were changed weekly. Mice had ad libitum access to municipal city water that was sterilized with ultraviolet light. Room temperature was maintained between 21°C and 23°C. Ear tags (#1005-1, National Band and Tag Co., Newport, KY, USA) were applied to pups at the time of genotyping for identification purposes. All animal procedures were approved by the Mayo Clinic Institutional Animal Care and Use Committee.

Statistical analysis

Prism software was used for statistical analysis and generation of survival, cataract, and tumor latency curves. Two-tailed unpaired *t* tests were used for pairwise significance unless otherwise indicated. Log-rank tests were used for survival, cataract, and tumor latency curves. For maximum lifespan extension analysis, two-sided Wang-Allison tests were used[14]. For consistency in these comparisons, the following denotes significance in all figures: * $P < 0.05$, ** $P < 0.01$ and *** $P < 0.001$. We note that no power calculations were used. Sample sizes were based on previously published experiments where differences were observed. No samples were excluded. Investigators were blinded to allocation during experiments and outcome assessment, except for rare instances where blinding was not possible.

Single-cell preparations and flow cytometry

To determine the cell type origin of senescent cells accumulating in fat, we prepared single-cells from iWAT, collected the stromal vascular fraction by centrifugation and labelled the

resulting cells with specific cell surface markers for collection of the $CD45^+$, endothelial, and progenitor (adipocyte stem cells + preadipocytes) cell populations by FACS as previously described[4, 35, 37]. To quantify progenitor cells, we divided the number progenitors recovered from the stromal vascular fraction by the total number of cells in the stromal vascular fraction. Single cell preparations from wounds were prepared in a similar manner. The proportion of GFP^+ cells in each population was assessed using flow cytometry as described[4].

Analysis of age-related phenotypes

Bi-weekly checks for cataracts were performed as described[5]. iWAT cell diameter, adipose depot weight, skin thickness, and skeletal muscle diameter measurements were as described[4]. Open field-testing was performed in a 50 cm × 50 cm box and analyzed with TopScan software (CleverSys Inc., Reston, VA, USA). Sclerotic glomeruli and BUN assessments were performed as described[38]. To determine cardiomyocyte cross-sectional area, three sagittal sections of the mid-ventricle separated by 400 um were stained with periodic acid-Schiff using a kit (Poly Scientific R&D, k098). At least 150 cardiomyocytes in the left ventricular free wall per section were measured using Image J software. Lethal isoproterenol challenges were performed as described[38]. Parameters of cardiac function were determined with echocardiography using Vevo2100 Imaging System (VisualSonics Inc., Toronto, Canada) with a 30 mHz transducer. Mice were lighly anesthetized by isoflurane (0.8–1.5%) with minimal effect on heart rate. Several m-mode recordings of the cardiac parasternal short axis at the level of papillary muscles were made and subsequently analyzed. For non-lethal isoproterenol challenge, mice were analyzed at baseline (day 0) and subsequently were administered five consecutive days of treatment with 10 $mg.kg^{-1}$ twice daily as described[39]. Mice were then assessed for alteration in LV mass on day 6. For longitudinal measurements of cardiac structure recordings were acquired in conscious animals. At least three different recordings per animal at each time point were analyzed. Rotarod assessments were as previously published[40]. Exercise ability was performed as described[4]. Novel object discrimination tests were performed as described[41]. Grip strength was determined as previously published[42]. Gross haematology was assessed by analysing EDTA-treated whole blood using a Hemavet 950 (Drew Scientific Inc., Miami Lakes, FL, USA). FACS-based analyses of peripheral blood leukocyte populations were as previously described[43]. $CD3^+$ T lymphocytes collected from peripheral blood (isolated using CD3 MicroBeads and MACS columns purchased from Miltenyi Biotec) according to manufacturers instructions. Glucose tolerance was assessed in mice fasted overnight by measuring blood glucose levels before and at timepoints after an intraperitoneal injection of glucose (1.0 $g.kg^{-1}$). Insulin sensitivity was measured following a 4 h fast by measuring blood glucose levels before and at timepoints after an intra-peritoneal injection of insulin (0.6 $mU.g^{-1}$). Serum IGF1 concentrations were measured by ELISA according to manufacturer's instructions (R&D Systems, catalog #MG100). Wound healing assessments were performed as previously described[44]. PTAH staining on formalin-fixed, paraffin-embedded tissue samples was performed as described previously[35].

Quantitative real-time PCR

RNA extraction, cDNA synthesis and qRT-PCR analysis of various mouse tissues and $CD3^+$ T lymphocytes collected from peripheral blood were performed as described[5]. RNA extraction from cell lines was performed according to manufacturer's instructions (Qiagen RNeasy mini kit). Sequences of primers for *FKBP-Casp8*, *EGFP*, $p16^{Ink4a}$, $p19^{Arf}$, *p21*, *Il-6*, *Pai1*, *Igfbp2* and *Mmp13* were as previously published[4]. In addition, the following primers were used: *Mmp3* forward 5′-CCTGATGT-TGGTGGCTTCA-3′, reverse 5′-TCCTGTAGGTGATGTGGGATTTC-3′; *Pparg* forward 5′-TCTTCCATCACGGAGAGGTC-3′, reverse 5′-GATGCACTGCCTATGAGC-AC-3′; *Cebpa* forward 5′-TTGTTTGGCTTTATCTCGGC-3′, reverse 5′-CCAAGAAG-TCGGTGGACAAG-3′; *Il1α* forward 5′-TCAACCAAACTATATATATCAGGATGT GG-3′, reverse 5′-CGAGTAGGCATACATGTCAAATTTTAC-3′; *Tnfα* forward 5′-AGGGTCTGGGCCATAGAACT-3′, reverse 5′-CAGCCTCTTCTCATTCCTGC-3′; *Agtr1a* forward 5′-AAGGGCCATTTTGCTTT-TCT-3′, reverse 5′-AACTCACAG-CAACCCTCCAA-3′; and *Abcc9 (Sur2a)* forward 5′-CAATG-GAGGCTGTCAGAACA -3′, reverse 5′-GGAGCTGACAGACACGAACA-3′. *Igfbp5* forward 5′-ATACAACCCAGAACGCCAGCT-3′, reverse 5′-ACCTGGGCTATGCACTTGATG-3′.

SA-β-Gal staining, electron microscopy and X-ray elemental analysis

For SA-β-Gal staining on kidney cryosections, tissue was embedded in OCT, sectioned at 10 μm thickness, and air-dried. Following rehydration in PBS, staining was performed using the Cell Signaling kit (#9860) with a 12-min fixation followed by incubating in the staining solution at 37°C for 12 h. Whole mount SA-β-Gal stainings on fat, kidney and heart were performed using a kit (Cell Signaling), with a 20-min fixation followed by immersing samples in the staining solution at 37°C for 12 h (iWAT and eWAT) or 48 h (heart and kidney). Detection of X-Gal crystals by transmission electron microscopy was as previously described[45]. Specifically, X-Gal-containing whole mounts were fixed in Trump's fixative at 4°C for 12 h and routinely processed for OsO_4/lead staining. Images were acquired and quantification performed on a Jeol 1400+ electron microscope with 80 kV acceleration voltage. The authenticity of X-Gal crystals was confirmed by X-ray elemental analysis, whereas the specificity of crystal formation was verified using fat and heart tissue that was not stained for SA-β-Gal. To measure the percentage of X-Gal-crystal-containing cells in kidney sections of AP- or vehicle-treated mice, we screened 5 grids (>1500 cells/grid) per treatment group for cells X-gal-positive cells at 3000× magnification. Cells with one or more crystals and the total number of cells were counted. iWAT and the visceral pericardium were assessed similarly, with cells with one or more crystals considered to be X-Gal positive. For iWAT, we only observed crystals in stromovascular cells with morphology and perivascular location consistent with adipocyte progenitors and therefore expressed the X-Gal fraction of total cells. >500 total fat cells per animal were scored for iWAT (n = 4 animals per group). Total cells was estimated by extrapolating from the cellularity of five 1500× fields. Due to dissection and processing, the serous pericardium was lost for most samples, so the visceral pericardium alone was scored via TEM. Only ciliated epithelial cells stained positive for SA-β-Gal, therefore we expressed the X-Gal positivity of this tissue as percentage of this cell type. The entire visible pericardium on one TEM grid per animal was scored, with 4

animals per group. For quantitation of SA-β-Gal positive cells in GFP^+ and GFP^- cell fractions collected from iWAT, 100 cells were scored per fraction (n = 3 animals).

Tissue immunofluorescence staining and western blotting

Paraffin-embedded kidney tissue sections (5 μm) were rehydrated (2× 10 min xylene; 2× 5 min 100% EtOH; 1× 5 min 95% EtOH; 1× 5 min 70% EtOH), incubated in protease from *Streptomyces griseus* (Sigma, P6911; 0.75 mg/ml in Tris buffer, 0.05 M, pH 7.6) for 1 h at 37°C to retrieve antigens, blocked with Rodent Block M (BioCare Medical) for 30 min, and incubated with rabbit anti-Agtr1a antibody (Novus Bio, NBP1-77078; 1:250) in antibody diluent (Dako) for 12 h at 4°C. Western blotting on tissue lysates was performed according to standard methods, incubating the nitrocellulose membrane overnight at 4°C with the following antibodies: Agtr1a (as above; 1:750), S6K (Cell Signaling, #2708; 1:1000), phospho-S6K (Cell Signaling, #9234; 1:1000), AKT (Cell Signaling, #9272; 1:1000), and phospho-AKT^{S473} (Cell Signaling, #9271; 1:1000). Quantification of p-S6K/S6K and p-AKT^{S473}/AKT ratios was performed as described[46, 47].

Cell culture

ATTAC MEFs were generated as previously described[4]. Western blotting for *p16*^{Ink4a} and mouse anti-actin was performed as described[48]. Growth curves were generated as previously described[48]. RNA extraction was done with a Micro RNeasy kit according to manufacturer's instructions (Qiagen). Early passage *p16-3MR* MEFs[8] were provided generously by Judith Campisi and Marco Demaria. Early passage homozygous *p16-FLUC* MEFs[49] were generously provided by Christin Burd. MEFs were immortalized by expression of SV40 large T antigen as described[50]. The cell line genotypes were authenticated by PCR genotyping. They were not tested for mycoplasma contamination.

Extended Data

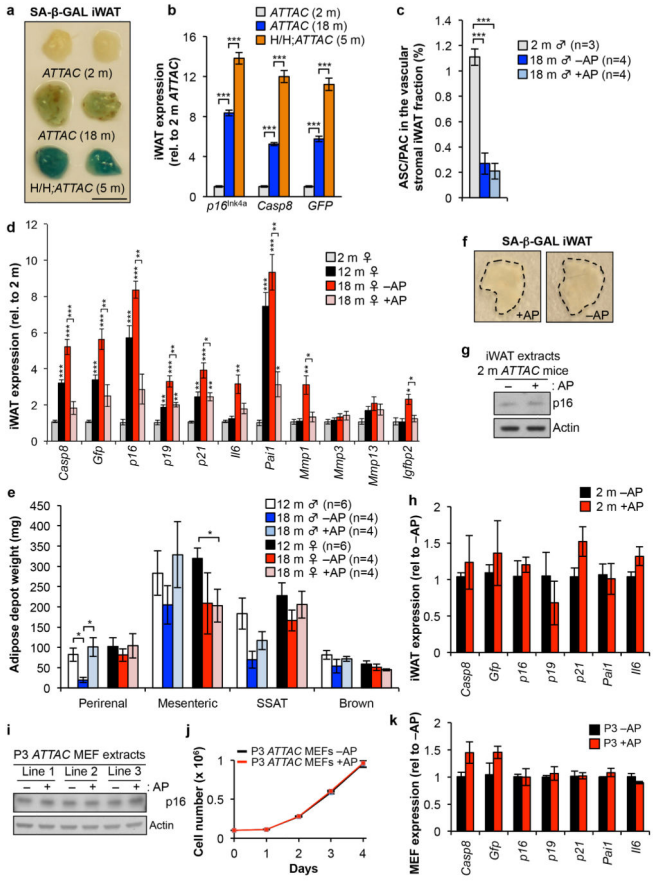

Extended Data Figure 1. *ATTAC* transgene expression tracks with expression of senescence markers in iWAT and induces apoptosis of senescent cells upon AP administration

a, Comparative analysis of SA-β-Gal activity in intact iWAT. **b**, Analysis of endogenous *p16*^{Ink4a} and *ATTAC* transcript SA-β-Gal activity in iWAT by qRT-PCR. Abbreviation: *H/H* (*BubR1*$^{H/H}$) (n = 4 mice per group). Scale bar, 0.5 cm. **c**, FACS-based quantitation of iWAT progenitor cell numbers in 18-month-old *ATTAC* mice treated with vehicle or AP. **d,** Expression of the *ATTAC* transgene and senescence markers in iWAT as determined by qRT-PCR (n = 4 mice per group). Asterisks above individual bars denote significant changes to 2-month-old mice; asterisks above brackets denote significant differences between 18-month-old vehicle and AP treated mice. **e,** Perirenal, mesenteric, subscapular and brown adipose depot weights. **f,** SA-β-Gal activity in iWAT from 2-month-old *ATTAC* mice treated with vehicle or AP beginning at weaning age. **g,** p16^{Ink4a} levels in iWAT from the mice described in **f**. Actin was used a loading control. **h,** Expression of *ATTAC* and senescence marker mRNA in the mice described in **f** (n = 3 mice per group). **(i–k)** Early passage non-senescent *ATTAC* MEFs express *p16*^{Ink4a} but are not susceptible to FKBP-Casp8-mediated elimination when cultured in the presence of AP. **i,** Levels of p16^{Ink4a} in passage 3 *ATTAC* mouse embryonic fibroblasts (MEFs), with and without AP treatment. **j,** Growth curves of passage 3 *ATTAC* MEFs (n =4 independently generated MEF lines per group), with and without AP treatment. **k,** Expression of *ATTAC* and senescence marker mRNA in passage 3

ATTAC MEFs (n = 3 independently generated MEF lines per group), with and without AP treatment. Error bars indicate s.e.m. Statistical significance was determined by unpaired two-tailed t tests. *, P<0.05; **, P<0.01; ***, P<0.001. For gel source data, see Supplementary Fig. 1.

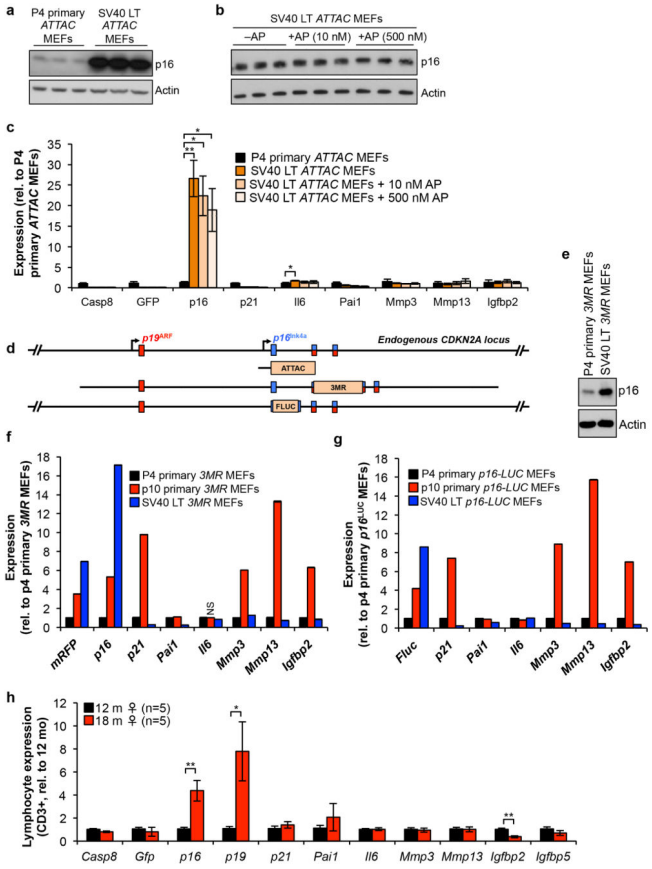

Extended Data Figure 2. *ATTAC* lacks promoter elements required for expression in replication competent cells or aged lymphocytes expressing high levels endogenous *p16*^{Ink4a}

(a–c) SV40 Large-T antigen-immortalized *ATTAC* MEFs robustly express endogenous *p16*^{Ink4a} (due to SV40 Large T-mediated inactivation of Rb) but fail to engage the *ATTAC* transgene and are not subject to FKBP-Casp8-mediated elimination. **a,** p16^{Ink4a} protein levels in p4 primary MEFs and MEFs immortalized with SV40 Large-T antigen. Actin was used as a loading control. **b**, p16^{Ink4a} protein levels in immortalized MEFs treated with vehicle or two concentrations of AP. Actin was used as a loading control. **c**, Expression of *ATTAC* and senescence marker transcripts in p4 primary MEFs, vehicle-treated immortalized MEFs, and AP-treated immortalized MEFs (n = 3 independently generated MEF lines per group). **d,** Schematic representation of the endogenous *p16*^{Ink4a} locus and the various *p16*^{Ink4a} promoter regions driving *ATTAC*, *3MR* and *Firefly luciferase* (*FLUC*). *ATTAC* and *p16-3MR* mice have 2.6 kb and ~50 kb *p16*^{Ink4a} promoter fragments driving transgene activity, respectively. *p16-FLUC* has firefly lucif-erase knocked into the endogenous *p16*^{Ink4a} locus, which keeps the entire promoter region intact but ablates p16^{Ink4a} protein expression. **e**, p16^{Ink4a} protein levels in early passage primary and SV40

Large-T antigen-immortalized *p16-3MR* MEFs. **f**, Expression of senescence marker mRNA in early and late passage primary MEFs and SV40 Large-T antigen-immortalized *p16-3MR* MEFs (n = 1 independently generated MEF line per group performed in triplicate). **g**, Expression of senescence marker mRNA in early and late passage primary MEFs and SV40 Large-T antigen-immortalized *p16-FLUC* MEFs (n = 1 independently generated MEF line per group performed in triplicate). **h**, Expression of *ATTAC* and senescence markers in $CD3^+$ T-cells from 12 and 18-month-old *ATTAC* mice (n = 5 mice per group). Error bars indicate s.e.m. Statistical significance was determined by unpaired two-tailed t tests. *, P<0.05; **, P<0.01; ***, P<0.001. We note that all values in **f** and **g** have a P<0.05 compared to p4 MEFs, with the exception of the one marked NS for not significant. For gel source data, see Supplementary Fig. 1.

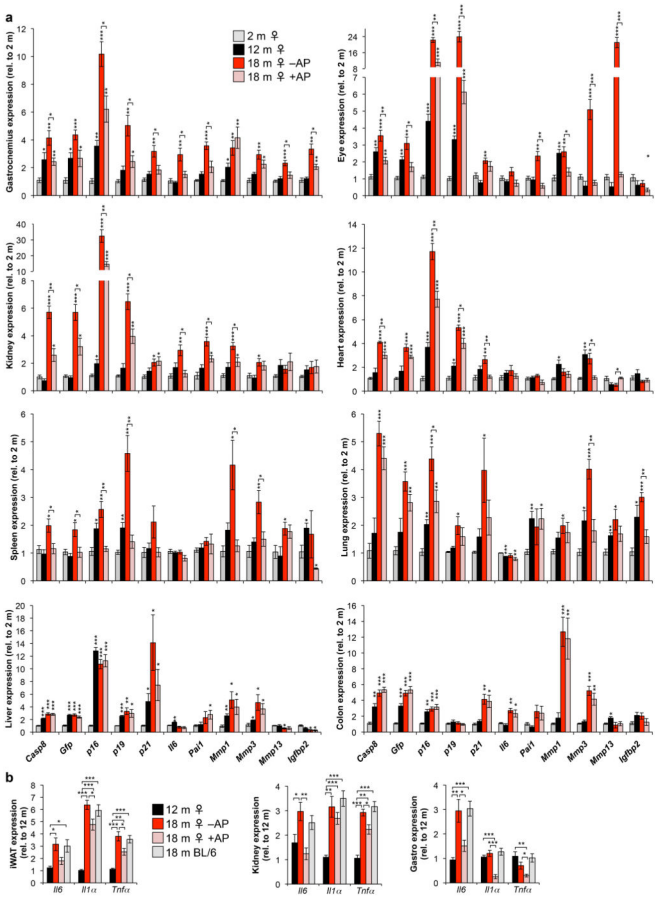

Extended Data Figure 3. *ATTAC*-mediated clearance of senescent cells is partial and tissue selective and attenuates expression of inflammation markers

a, Expression of the *ATTAC* transgene and a senescence marker panel, as determined by RT-PCR, in gastrocnemius, eye, kidney, heart (atria), spleen, lung, liver, and colon (n = 4 females per group). **b,** Expression of *Il6*, *Il1a* and *Tnfa* as determined by qRT-PCR in mouse iWAT, kidney and skeletal muscle at different ages (n = 4 females per group). *Il6* values are as indicated in Extended Data Fig. 1d (iWAT) and 3a (kidney and gastrocnemius). Expression levels of inflammation markers in unmanipulated 18-month-old C57BL/6

females suggests that repeated vehicle injections were not a source of tissue inflammation. Error bars indicate s.e.m. Statistical significance was determined by unpaired two-tailed t tests. *, $P<0.05$; **, $P<0.01$; ***, $P<0.001$. Asterisks above individual bars in (**a**) denote significant changes to 2-month-old mice; asterisks above brackets denote significant differences between 18-month-old vehicle and AP treated mice.

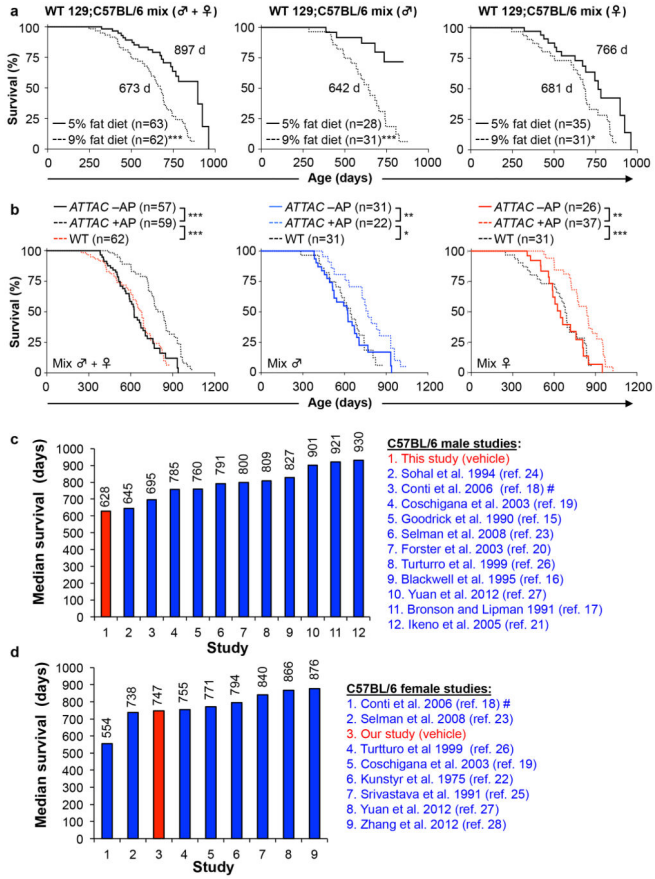

Extended Data Figure 4. Comparison of lifespans under different diets and housing facilities

a, Survival curves of unmanipulated wild-type 129Sv-C57BL/6 mice fed a 5% versus 9% fat diet. Median lifespan (in days) are indicated. **b**, Survival curves of unmanipulated wild-type 129Sv-C57BL/6 mice fed 9% fat diet plotted against those of vehicle- (-AP) and AP-treated (+AP) 129Sv-C57BL/6-FVB *ATTAC* mice from Fig. 2b. These data suggest that the lifespans of vehicle-injected 129Sv-C57BL/6-FVB control mice were quite normal for the diet that they were on and unlikely to be negatively impacted by repeated intraperitoneal injections. Log-rank tests were used to determine statistical significance. *, $P<0.01$; ** $P<0.001$; ***, $P<0.001$. **c**, **d**, Median survival data of unmanipulated C57BL/6 male (**c**) and female (**d**) mice from various laboratories for comparsion to the results obtained from our facility.

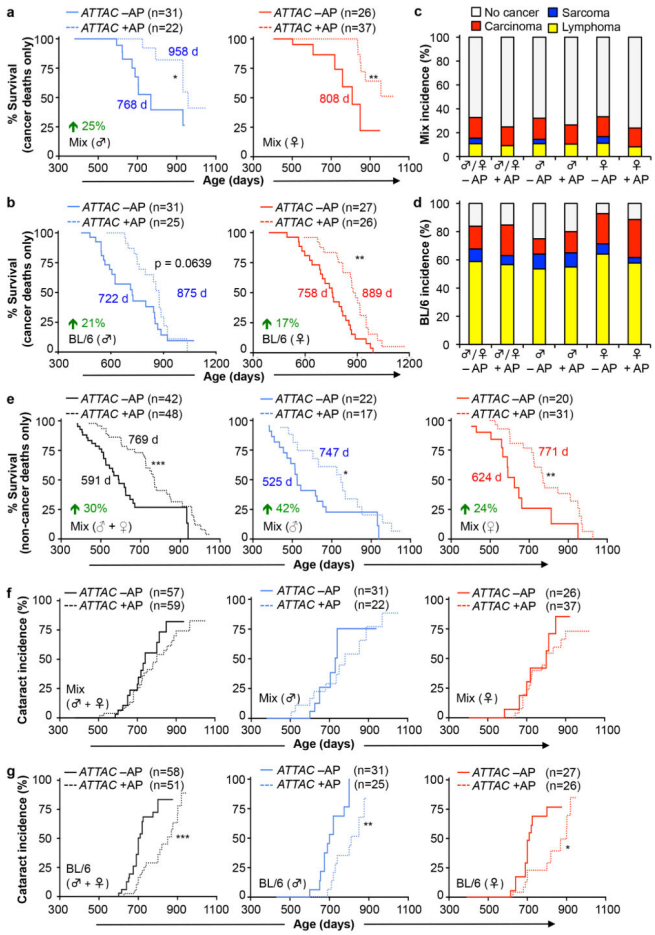

Extended Data Figure 5. Senescent cell clearance increases delays tumor and cataract formation

a, **b**, Survival curves of mixed (**a**) and C57BL/6 (**b**) *ATTAC* mice dying of cancer (mice that had an overt tumor at time of death; only mice with lymphomas, sarcomas and carcinomas were included). Median survival (in days) and percentage increase are indicated. **c**, **d,** Incidence of macroscopically detectable neoplasms (lymphomas, sarcomas and carcinomas) at time of death in mixed (**c**) and C57BL/6 (**d**) *ATTAC* mice from survival cohorts. **e**, Survival curves of C57BL/6-129Sv-FVB mice dying without cancer (mice that had an overt tumor at time of death, including lymphoma, sarcoma and/or carcinoma, were excluded). Median survival (in days) and percentage increase are indicated. **f**–**g,** Cataract incidence for mixed (**f**) and C57BL/6 (**g**) *ATTAC* mouse cohorts. Log-rank tests were used to determine statistical significance in **a**, **b**, and **e**–**g**. *, $P<0.05$; **, $P<0.01$; ***, $P<0.001$.

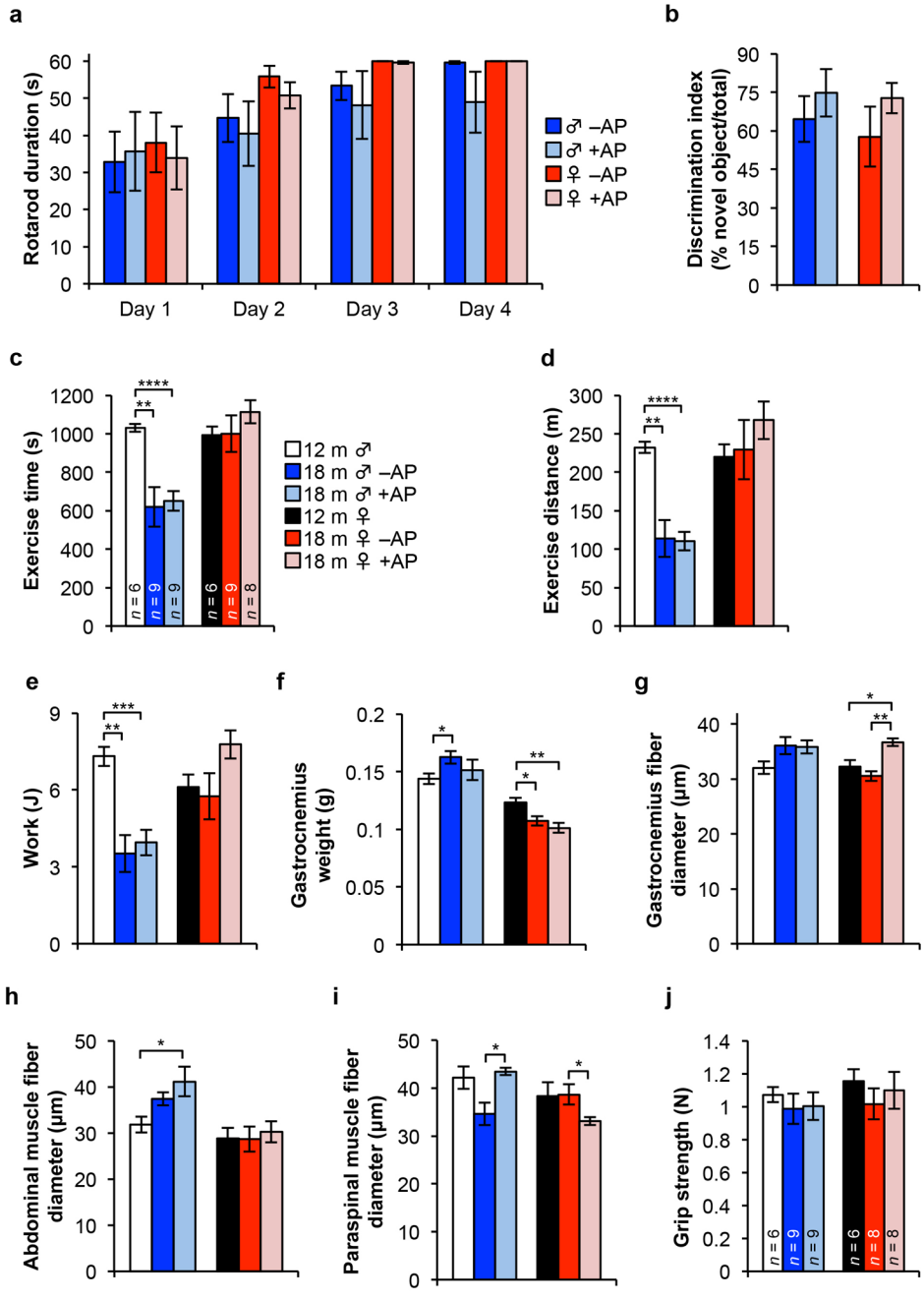

Extended Data Figure 6. Senescent cell clearance does not affect coordination, memory or exercise ability of 18-month-old *ATTAC* mice

a, Time spent balanced during a fixed speed rotarod test for 18-month-old *ATTAC* mice (*n* = 6 male and 8 female mice per group). **b,** Novel object investigation test. The percent of investigations of a novel object divided by the total investigations is graphed. Key and animal numbers are as indicated in **a. c–e**, Time-to-exhaustion (**c**), distance (**d**) and work (**e**) during a treadmill exercise test. Animal numbers are as indicated in **c. f**, Gastrocnemius muscle weight of *ATTAC* mice (*n* = 6 12-month-old males and females; *n*= 4 18-month-old –AP males and females; *n* = 4 18-month-old +AP males and females). **g–i,** Myofiber

diameter measurements on isolated gastrocnemius (**g**), abdominal (**h**), and paraspinal muscle (**i**). Animal numbers are as indicated in **f. j**, Analysis of forelimb grip strength of *ATTAC* mice. Legends in **d–j** are as in **c**. Error bars indicate s.e.m. Unpaired two-tailed t tests were used to determine statistical significance. *, $P<0.05$; **, $P<0.01$; ***, $P<0.001$.

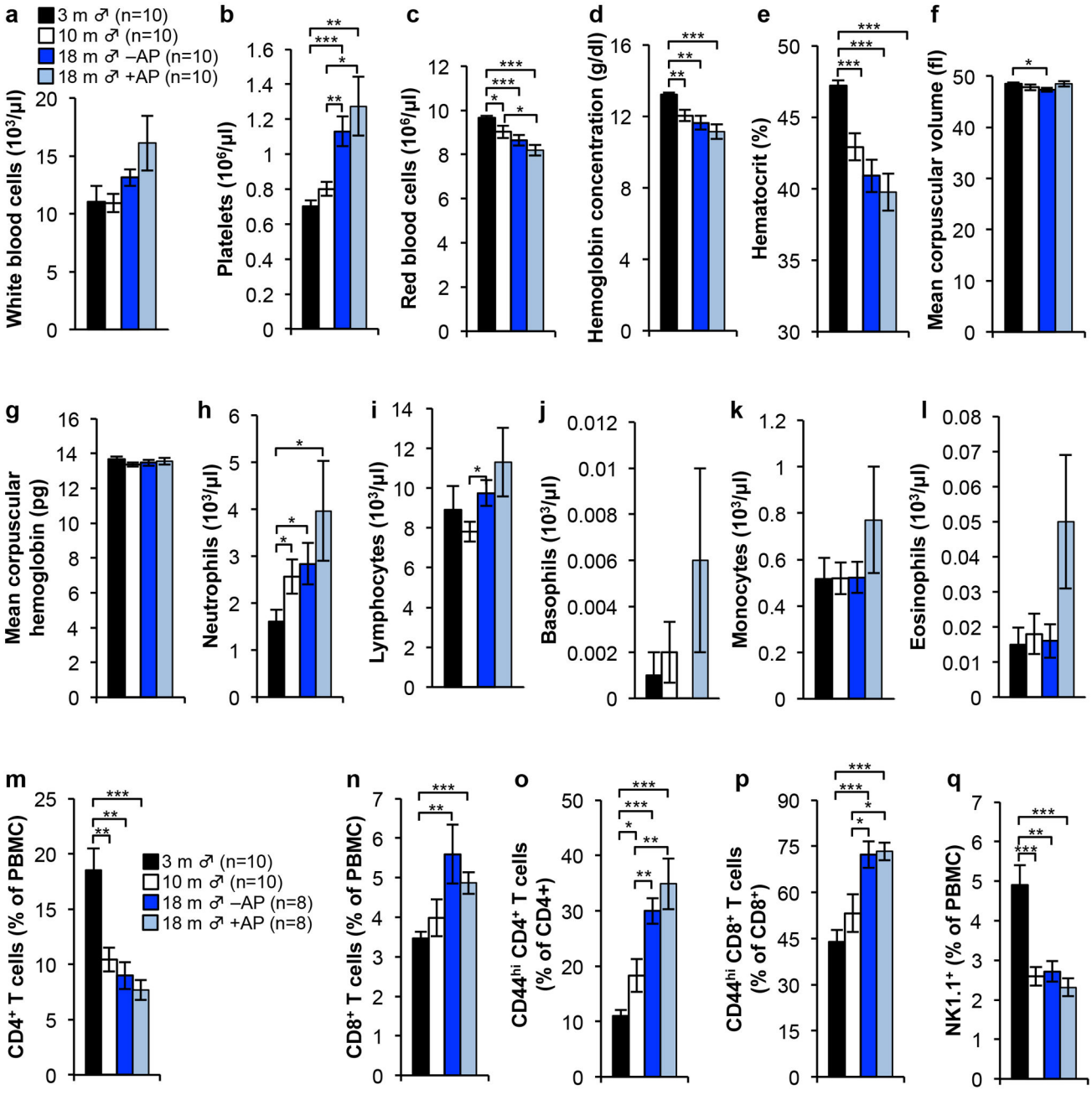

Extended Data Figure 7. Senescent cell clearance has no impact on hematological parameters and age-related changes in leukocyte populations

a–l, Hematology results of 3-, and 10-month-old untreated *ATTAC* C57BL/6 mice and 18-month-old vehicle and AP treated *ATTAC* C57BL/6 mice. White blood cell count (**a**),

platelet count (**b**), red blood cell count (**c**), hemaglobin concentration (**d**), haematocrit (**e**), mean corpuscular volume (**f**), mean corpuscular haemoglobin (**g**), neutrophils (**h**), lymphocyptes (**i**), basophils (**j**), monocytes (**k**), and eosinophils (**l**). **(m–q)**, Assessment for leukocyte subpopulations in 3-, and 10-month-old untreated *ATTAC* C57BL/6 mice and 18-month-old vehicle and AP treated *ATTAC* C57BL/6 mice. $CD4^+$ T cells (% of peripheral blood mononuclear cells or PBMC) (**m**), $CD8^+$ T cells (% of PBMC) (**n**), $CD44^{hi}$ $CD4^+$ T cells (% of $CD4^+$) (**o**), $CD44^{hi}$ $CD8^+$ T cells (% of $CD8^+$) (**p**), and $NK1.1^+$ cells (% of PBMC) (**q**). Key and animal numbers in **b–l** are as indicated in **a**, key and animal numbers in **n–q** are as indicated in **m**. Error bars indicate s.e.m. Unpaired two-tailed t tests were used to determine statistical significance. *, $P<0.05$; **, $P<0.01$; ***, $P<0.001$.

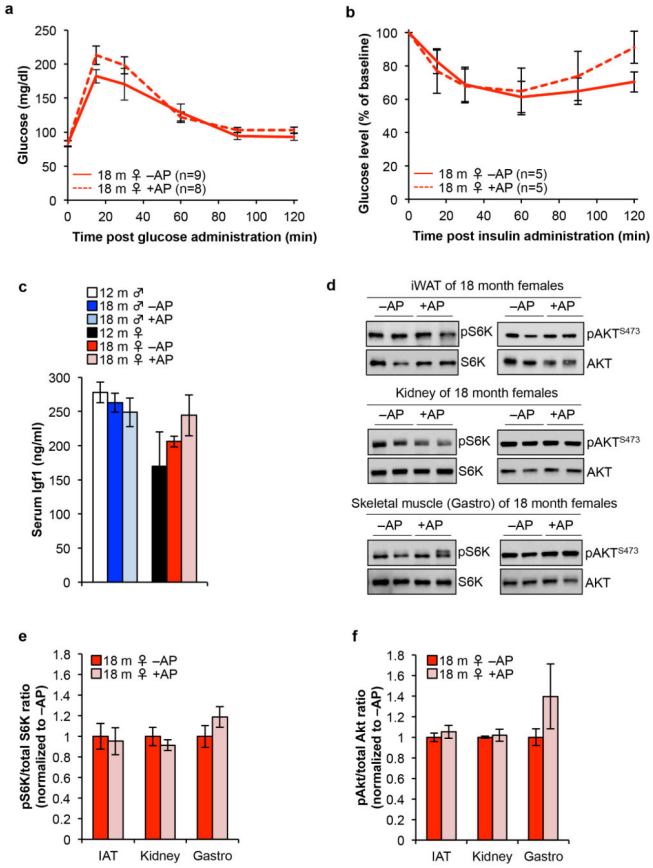

Extended Data Figure 8. Senescent cell removal does not impact somatotrophic axis signaling in vivo

a, Glucose levels following intraperitoneal glucose administration following an overnight fast in 18-month-old vehicle- and AP-treated *ATTAC* C57BL/6 females. **b,** Normalized glucose levels following intraperitoneal insulin administration following a 4 hour fast in 18-month-old vehicle- and AP-treated *ATTAC* C57BL/6 females. **c,** Serum Igf1 levels in *ATTAC* C57BL/6 mice ($n = 4$ mice of each group). **d,** Representative western blots for phospho-S6K, total S6K, phospho-AKT^{S473} and total AKT in iWAT, kidney and skeletal muscle tissue lysates from 18-month-old vehicle- and AP-treated *ATTAC* C57BL/6 females. Serum Igf1 levels in *ATTAC* C57BL/6 mice ($n = 4$ mice of each group). **e,** Quantification of

phospho-S6K to total S6K ratio in blots from (**d**), $n = 4$ mice of each group. **f,** Quantification of phospho-AKT^{S473} to total AKT ratio in blots from (**d**), $n = 4$ mice of each group. Error bars indicate s.e.m. No statistically significant differences were observed in **a–c** and **e–f** using unpaired two-tailed t tests. For gel source data, see Supplementary Fig. 1.

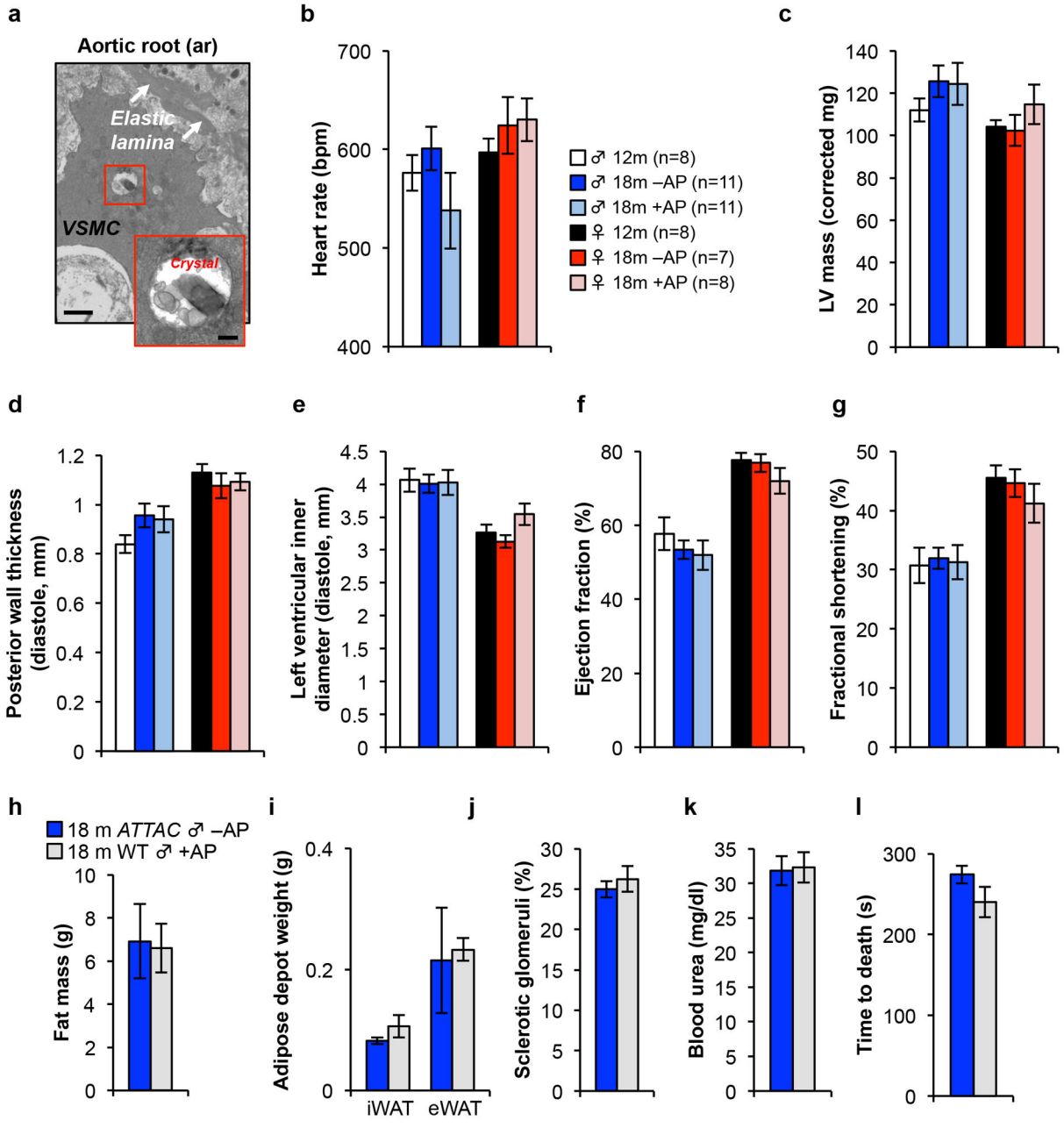

Extended Data Figure 9. Senescent cell clearance does not alter cardiac morphology and function in "resting" mice and AP treatment has no impact on healthspan of mice lacking the *ATTAC* transgene

a, Electron micrographs of X-Gal crystal containing cells in the aortic root. *VSMC*, vascular smooth muscle cell. Scale bars, 1 μm (main panel) and 200 nm (inset). **(b–g)**

Echocardiography measurements of heart rate (**b**), left ventricular mass (**c**), posterior wall thickness (**d**), left ventricular inner diameter (**e**), ejection fraction (**f**), and the fractional shortening of the heart (**g**) in 12-month-old untreated mice and 18-month-old *ATTAC* mice treated with vehicle or AP. **h**, Fat mass (n = 9 mice per group). 18-month-old *ATTAC* vehicle treated mouse values are the same as indicated in Fig. 1. **i**, iWAT and eWAT depot weight (n = 4 mice per group). 18-month-old *ATTAC* vehicle treated mouse values are the same as indicated in Fig. 1. **j**, **k**, Kidney sclerosis (**j**) and blood urea levels (**k**) (n = 4 mice per group). 18-month-old *ATTAC* vehicle treated mouse values are the same as indicated in Fig. 4. **l**, Time to death following isoproterenol administration (n = 4 mice per group). 18-month-old *ATTAC* vehicle treated mouse values are the same as indicated in Fig. 5. Legends and number of animals in **c–g** are as in **b**, legends in **i–l** are as in **h**. Error bars indicate s.e.m. No statistically significant differences were observed using unpaired two-tailed t tests.

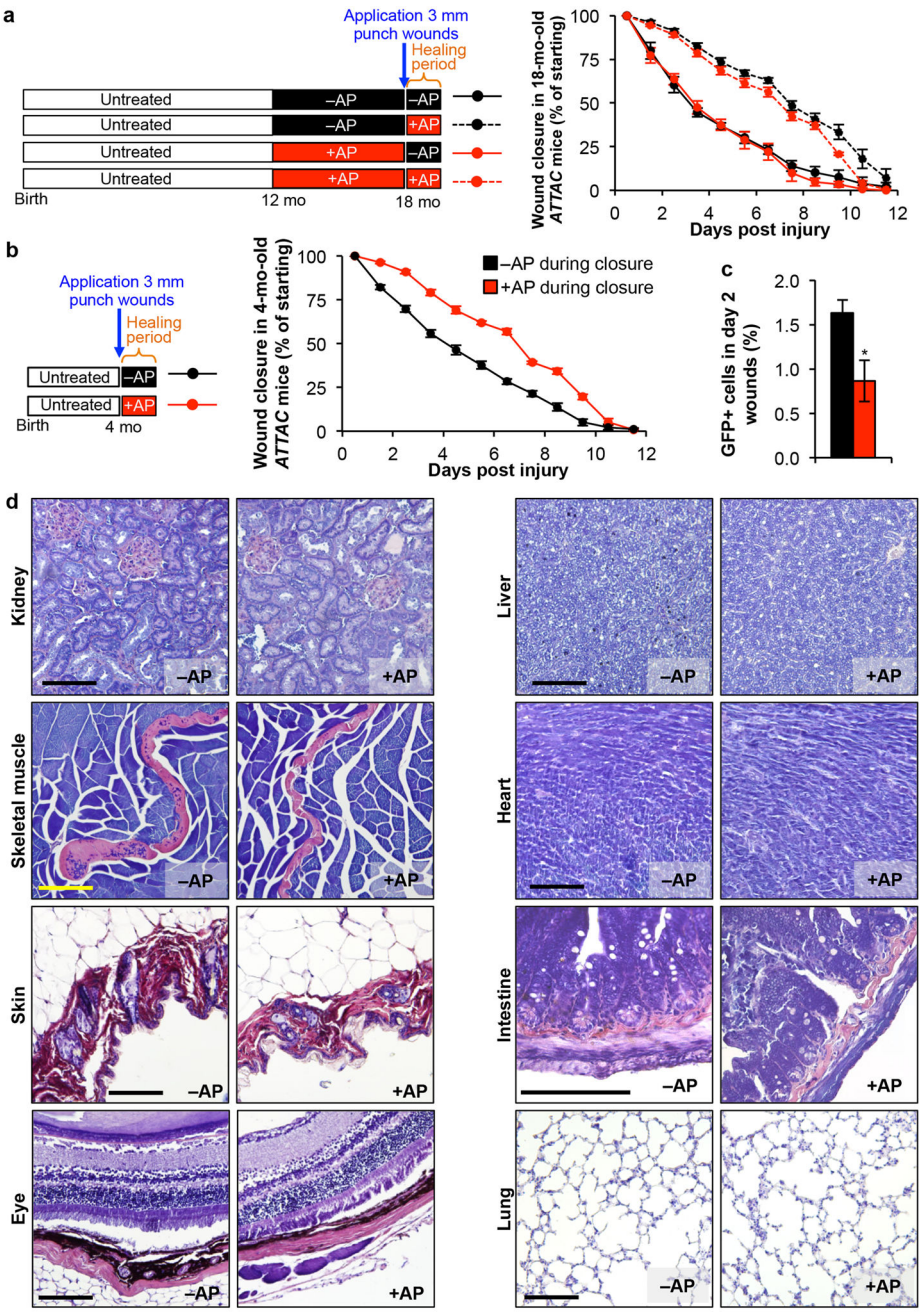

Extended Data Figure 10. Impact of senescent cell clearance on wound healing and tissue fibrosis

a, Closure of 3-mm punch biopsy wounds in 18-month-old *ATTAC* females after treatment with vehicle or AP for 6 months and if drug treatment was stopped 2 days prior to skin puncture or continued during wound closure (n = 6 wounds for –AP;–AP and +AP;–AP and n = 10 wounds for –AP;+AP and +AP;+AP). AP administration during the wound healing process significantly attenuates the rate of wound closure independently of whether senescent cell removal had occurred prior to wounding. **b**, Closure of 3-mm punch biopsy wounds in 4-month-old *ATTAC* females after treatment with vehicle or AP following wounding (n = 10 wounds per group). Similar to 18-month-old mice, AP administration

during the wound healing process dramatically attenuated the rate of wound closure. **c**, Quantification of total GFP^+ cells isolated from 3-mm punch biopsy wounds of 4-month-old mice two days into the wound healing process treated with vehicle (black) or AP (red, $n = 3$ mice per group). **d**, PTAH-stained tissues sections from 18-month-old *ATTAC* mice for detection of fibrosis. Scale bars, 100 μm. Error bars indicate s.e.m. Unpaired two-tailed t tests were used to determine statistical significance for **a–c**. Mice receiving AP during the healing process in **a** and **b** are significantly different from those treated with vehicle from day 1.5 through day 9.5. *, $P<0.05$.

Supplementary Material

Refer to Web version on PubMed Central for supplementary material.

Acknowledgments

We thank Masakazu Hamada, John Rainey, Qianqian Guo, Svetlana Bornschlegl, Ming Li, Carolyn M. Roos, Naomi Hamada, and Bin Zhang for assistance and Christin Burd, Santiago Reyes Ramirez, Paul Galardy, and David Katzmann and the members of Program Project Grant AG041122 for helpful discussions. We are very grateful to Richard Miller and Steve Austad for help with the design and interpretation of our lifespan studies. We thank Christin Burd and Judith Campisi for sharing *p16*^{Ink4a}-LUC and *3MR* MEFs, respectively. This work was supported by the National Institutes of Health (J.M.v.D. R01CA96985 and AG041122 project 1) and (J.D.M., HL111121), the Paul F. Glenn Foundation (J.M.v.D. and D.J.B.), the Ellison Medical Foundation (D.J.B.), the Noaber Foundation (J.M.v.D.), the Children's Research Center (D.J.B.) and the Robert and Arlene Kogod Center on Aging (D.J.B.).

References

1. Campisi J. Aging, cellular senescence, and cancer. Annual review of physiology. 2013; 75:685–705.
2. Sharpless NE, Sherr CJ. Forging a signature of in vivo senescence. Nat Rev Cancer. 2015; 15:397–408. [PubMed: 26105537]
3. van Deursen JM. The role of senescent cells in ageing. Nature. 2014; 509:439–446. [PubMed: 24848057]
4. Baker DJ, et al. Clearance of p16Ink4a-positive senescent cells delays ageing-associated disorders. Nature. 2011; 479:232–236. [PubMed: 22048312]
5. Baker DJ, et al. Opposing roles for p16Ink4a and p19Arf in senescence and ageing caused by BubR1 insufficiency. Nature cell biology. 2008; 10:825–836. [PubMed: 18516091]
6. Jun JI, Lau LF. The matricellular protein CCN1 induces fibroblast senescence and restricts fibrosis in cutaneous wound healing. Nat Cell Biol. 2010; 12:676–685. [PubMed: 20526329]
7. Krizhanovsky V, et al. Senescence of activated stellate cells limits liver fibrosis. Cell. 2008; 134:657–667. [PubMed: 18724938]
8. Demaria M, et al. An Essential Role for Senescent Cells in Optimal Wound Healing through Secretion of PDGF-AA. Dev Cell. 2014; 31:722–733. [PubMed: 25499914]
9. Munoz-Espin D, et al. Programmed Cell Senescence during Mammalian Embryonic Development. Cell. 2013; 155:1104–1118. [PubMed: 24238962]
10. Storer M, et al. Senescence Is a Developmental Mechanism that Contributes to Embryonic Growth and Patterning. Cell. 2013; 155:1119–1130. [PubMed: 24238961]
11. Wang W, Wu J, Zhang Z, Tong T. Characterization of regulatory elements on the promoter region of p16(INK4a) that contribute to overexpression of p16 in senescent fibroblasts. J Biol Chem. 2001; 276:48655–48661. [PubMed: 11598130]
12. Tchkonia T, et al. Fat tissue, aging, and cellular senescence. Aging cell. 2010; 9:667–684. [PubMed: 20701600]
13. Liu Y, et al. Expression of p16(INK4a) in peripheral blood T-cells is a biomarker of human aging. Aging Cell. 2009; 8:439–448. [PubMed: 19485966]

14. Wang C, Li Q, Redden DT, Weindruch R, Allison DB. Statistical methods for testing effects on "maximum lifespan". Mech Ageing Dev. 2004; 125:629–632. [PubMed: 15491681]
15. Goodrick CL, Ingram DK, Reynolds MA, Freeman JR, Cider N. Effects of intermittent feeding upon body weight and lifespan in inbred mice: interaction of genotype and age. Mech Ageing Dev. 1990; 55:69–87. [PubMed: 2402168]
16. Blackwell BN, Bucci TJ, Hart RW, Turturro A. Longevity, body weight, and neoplasia in ad libitum-fed and diet-restricted C57BL6 mice fed NIH-31 open formula diet. Toxicol Pathol. 1995; 23:570–582. [PubMed: 8578100]
17. Bronson RT, Lipman RD. Reduction in rate of occurrence of age related lesions in dietary restricted laboratory mice. Growth Dev Aging. 1991; 55:169–184. [PubMed: 1765417]
18. Conti B, et al. Transgenic mice with a reduced core body temperature have an increased life span. Science. 2006; 314:825–828. [PubMed: 17082459]
19. Coschigano KT, et al. Deletion, but not antagonism, of the mouse growth hormone receptor results in severely decreased body weights, insulin, and insulin-like growth factor I levels and increased life span. Endocrinology. 2003; 144:3799–3810. [PubMed: 12933651]
20. Forster MJ, Morris P, Sohal RS. Genotype and age influence the effect of caloric intake on mortality in mice. FASEB J. 2003; 17:690–692. [PubMed: 12586746]
21. Ikeno Y, et al. Housing density does not influence the longevity effect of calorie restriction. J Gerontol A Biol Sci Med Sci. 2005; 60:1510–1517. [PubMed: 16424282]
22. Kunstyr I, Leuenberger HG. Gerontological data of C57BL/6J mice. I. Sex differences in survival curves. J Gerontol. 1975; 30:157–162. [PubMed: 1123533]
23. Selman C, et al. Evidence for lifespan extension and delayed age-related biomarkers in insulin receptor substrate 1 null mice. FASEB J. 2008; 22:807–818. [PubMed: 17928362]
24. Sohal RS, Ku HH, Agarwal S, Forster MJ, Lal H. Oxidative damage, mitochondrial oxidant generation and antioxidant defenses during aging and in response to food restriction in the mouse. Mech Ageing Dev. 1994; 74:121–133. [PubMed: 7934203]
25. Srivastava VK, Tilley RD, Hart RW, Busbee DL. Effect of dietary restriction on the fidelity of DNA polymerases in aging mice. Exp Gerontol. 1991; 26:453–466. [PubMed: 1756777]
26. Turturro A, et al. Growth curves and survival characteristics of the animals used in the Biomarkers of Aging Program. J Gerontol A Biol Sci Med Sci. 1999; 54:B492–501. [PubMed: 10619312]
27. Yuan R, et al. Genetic coregulation of age of female sexual maturation and lifespan through circulating IGF1 among inbred mouse strains. Proc Natl Acad Sci U S A. 2012; 109:8224–8229. [PubMed: 22566614]
28. Zhang Y, et al. The starvation hormone, fibroblast growth factor-21, extends lifespan in mice. Elife. 2012; 1:e00065. [PubMed: 23066506]
29. Richardson A, et al. Measures of Healthspan as Indices of Aging in Mice-A Recommendation. J Gerontol A Biol Sci Med Sci. 2015
30. Razzaque MS. Does renal ageing affect survival? Ageing Res Rev. 2007; 6:211–222. [PubMed: 17662672]
31. Ferder LF, Inserra F, Basso N. Effects of renin-angiotensin system blockade in the aging kidney. Exp Gerontol. 2003; 38:237–244. [PubMed: 12581787]
32. Paul M, Poyan Mehr A, Kreutz R. Physiology of local renin-angiotensin systems. Physiol Rev. 2006; 86:747–803. [PubMed: 16816138]
33. Bernhard D, Laufer G. The aging cardiomyocyte: a mini-review. Gerontology. 2008; 54:24–31. [PubMed: 18196923]
34. Sudhir R, Sukhodub A, Du Q, Jovanovic S, Jovanovic A. Ageing-induced decline in physical endurance in mice is associated with decrease in cardiac SUR2A and increase in cardiac susceptibility to metabolic stress: therapeutic prospects for up-regulation of SUR2A. Biogerontology. 2011; 12:147–155. [PubMed: 20972622]
35. Baker DJ, et al. Increased expression of BubR1 protects against aneuploidy and cancer and extends healthy lifespan. Nat Cell Biol. 2012
36. Childs BG, Durik M, Baker DJ, van Deursen JM. Cellular senescence in aging and age-related disease: from mechanisms to therapy. Nat Med. 2015; 21:1424–1435. [PubMed: 26646499]

37. Baker DJ, Weaver RL, van Deursen JM. p21 both attenuates and drives senescence and aging in BubR1 progeroid mice. Cell reports. 2013; 3:1164–1174. [PubMed: 23602569]
38. Baker DJ, et al. Increased expression of BubR1 protects against aneuploidy and cancer and extends healthy lifespan. Nat Cell Biol. 2012; 15:96–102. [PubMed: 23242215]
39. Zingman LV, et al. Kir6.2 is required for adaptation to stress. Proc Natl Acad Sci U S A. 2002; 99:13278–13283. [PubMed: 12271142]
40. Wijshake T, et al. Reduced Life- and Healthspan in Mice Carrying a Mono-Allelic BubR1 MVA Mutation. PLoS Genet. 2012; 8:e1003138. [PubMed: 23300461]
41. Buenz EJ, et al. Apoptosis of hippocampal pyramidal neurons is virus independent in a mouse model of acute neurovirulent picornavirus infection. Am J Pathol. 2009; 175:668–684. [PubMed: 19608874]
42. Maskey RS, et al. Spartan deficiency causes genomic instability and progeroid phenotypes. Nat Commun. 2014; 5:5744. [PubMed: 25501849]
43. Blatner NR, et al. Expression of RORgammat marks a pathogenic regulatory T cell subset in human colon cancer. Science translational medicine. 2012; 4:164ra159.
44. Baker DJ, et al. BubR1 insufficiency causes early onset of aging-associated phenotypes and infertility in mice. Nat Genet. 2004; 36:744–749. [PubMed: 15208629]
45. Stollewerk A, Klambt C, Cantera R. Electron microscopic analysis of Drosophila midline glia during embryogenesis and larval development using beta-galactosidase expression as endogenous cell marker. Microscopy research and technique. 1996; 35:294–306. [PubMed: 8956276]
46. Garelick MG, et al. Chronic rapamycin treatment or lack of S6K1 does not reduce ribosome activity in vivo. Cell Cycle. 2013; 12:2493–2504. [PubMed: 23839034]
47. Schreiber KH, et al. Rapamycin-mediated mTORC2 inhibition is determined by the relative expression of FK506-binding proteins. Aging Cell. 2015; 14:265–273. [PubMed: 25652038]
48. Baker DJ, et al. BubR1 insufficiency causes early onset of aging-associated phenotypes and infertility in mice. Nature genetics. 2004; 36:744–749. [PubMed: 15208629]
49. Burd CE, et al. Monitoring Tumorigenesis and Senescence In Vivo with a p16(INK4a)-Luciferase Model. Cell. 2013; 152:340–351. [PubMed: 23332765]
50. Ricke RM, Jeganathan KB, Malureanu L, Harrison AM, van Deursen JM. Bub1 kinase activity drives error correction and mitotic checkpoint control but not tumor suppression. The Journal of cell biology. 2012; 199:931–949. [PubMed: 23209306]

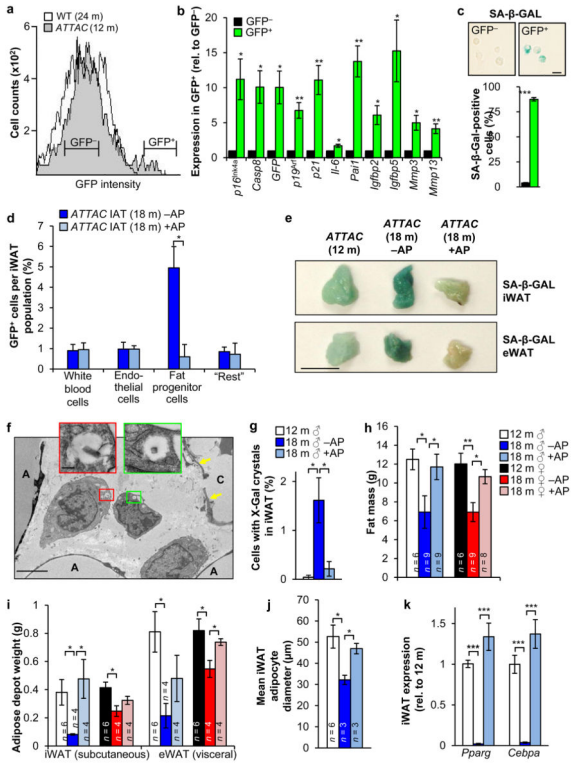

Figure 1. Clearance of senescent fat progenitor cells attenuates age-related lipodystrophy

a, FACS profiles of single-cell suspensions from iWAT of the indicated mice. **b**, GFP$^+$ and GFP$^-$ cell populations from iWAT of 12-month-old *ATTAC* mice (see **a** for sorting brackets) analyzed by qRT-PCR (n = 6 mice). **c**, SA-β-Gal activity in GFP$^+$ and GFP$^-$ iWAT cells (n = 3 mice). **d,** GFP$^+$ cells in the indicated iWAT cell populations ("Rest" represents the iWAT vascular stromal fraction minus leukocytes, endothelial cells and progenitors). **e–i**, Fat-related analyses on C57BL/6 *ATTAC* mice prior to treatment (12 m) or after 6 months of treatment with vehicle (18 m –AP) or AP (18 m +AP). **e**, SA-β-Gal activity in iWAT (IAT) and eWAT (epididiymal). **f**, Electron micrograph showing perivascular X-Gal-positive cells from an 18-month-old vehicle-treated C57BL/6 *ATTAC* male. A, adipocyte; C, capillary. Arrows mark endothelial cells. **g**, Quantitation of iWAT cells containing X-Gal crystals (n = 4 mice per treatment). **h**, Fat mass measurements. **i**, iWAT and eWAT depot weights. **j**, Mean adipocyte diameters in iWAT. **k**, Expression of adipogenesis markers in iWAT (n = 4 mice per group). Scale bars: 10 μm in **c**; 0.5 cm in **e**; 2 μm in the main panel of **f** and 200 nm in the insets. Legends in **i–k** are as in **h**. Error bars indicate s.e.m. Statistical significance in **b** was determined by one sample t tests using a theoretical mean of 1, and by unpaired two-tailed t tests in all other panels. *, P<0.05; **, P<0.01; ***, P<0.001.

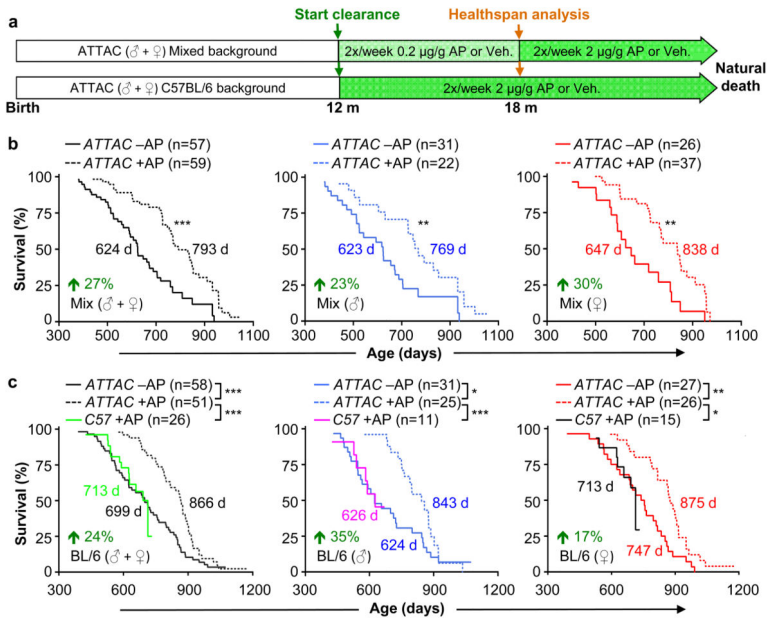

Figure 2. Senescent cell clearance extends lifespan

a, Study design for clearance of senescent cells in mixed and C57BL/6 mouse cohorts. Healthspan analysis was done at 18 months, an age where relatively few mice in vehicle (Veh)- or AP-treated have died and bias due to selection for long-lived animals is unlikely. **b**, **c**, Survival curves for vehicle- (–AP) and AP-treated (+AP) mixed (**b**) and C57BL/6 mice (**c**). Median survival (in days) and percentage increase in median survival are indicated. We note that median lifespans of our vehicle-treated cohorts are similar to those of wild-type mice administered AP (**c**). Log-rank tests were used to determine statistical significance. *, $P<0.05$; **, $P<0.01$; ***, $P<0.001$.

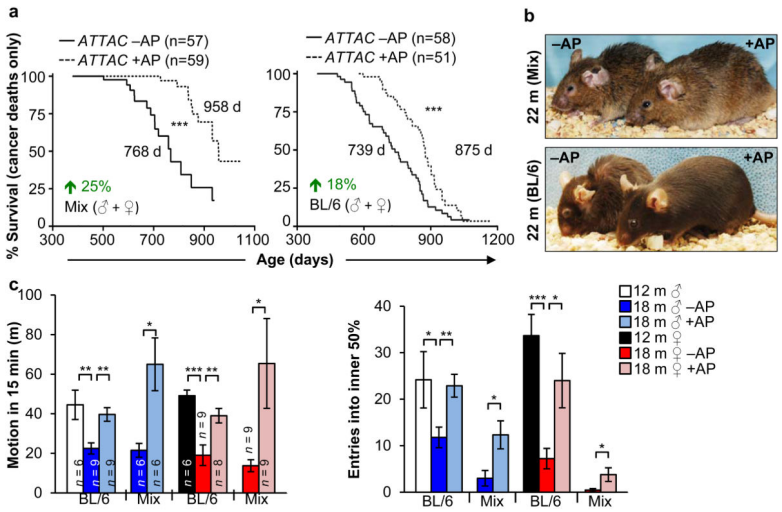

Figure 3. Clearance of senescent cells prolongs healthspan

a, Survival curves of *AT-TAC* mice dying of cancer (mice that had an overt tumor at time of death; mice with lymphomas, sarcomas and carcinomas were included, mice without tumors were censored). Median survival and percentage increase are indicated. **b**, Representative images of aged mice with and without senescent cell clearance. **c**, Spontaneous movement and exploratory behavior of *ATTAC* mice analyzed by the open field test. Error bars indicate s.e.m. Log-rank tests were used to determine statistical significance in **a**; unpaired two-tailed t tests were used in **c**. *, $P<0.05$; **, $P<0.01$; ***, $P<0.001$.

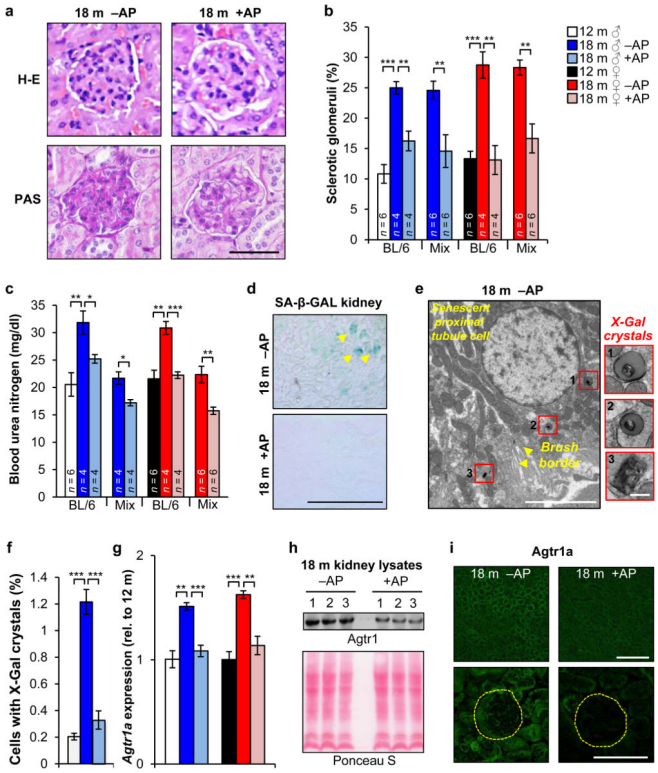

Figure 4. Senescent cells cause glomerulosclerosis, kidney dysfunction and renal RAAS hyperactivity

a, Images of sclerotic (left) and normal (right) glomeruli from the indicated mice. **b**, Quantification of sclerotic glomeruli. **c**, Measurements of blood urea nitrogen levels. **d**, SA-β-Gal-stained kidney sections. **e**, Electron micrograph showing a X-Gal crystal-containing renal epithelial cell with brush border membrane (arrowheads). Insets show X-Gal crystal close-ups. **f**, Percent of cells with X-Gal crystals in renal sections (n = 5 TEM grids for each treatment group). **g**, Renal expression of *Agtr1a* analyzed by qRT-PCR (n = 4 mice per group). **h**, Western blot of kidney lysates probed for Agtr1a (n = 3 mice per treatment group). Ponceau S staining served as loading control. **i**, Immunostaining of kidney sections for Agtr1a. Yellow circles denotes glomeruli. Scale bars: 50 μm in **a**; 250 μm in **d**; 5 μm (main panel) and 200 nm (insets) in **e;** 100 μm (top) and 50 μm (bottom) in **i**. Legends in **c**, **f** and **g** are as in **b**. Error bars indicate s.e.m. Statistical significance was determined by unpaired two-tailed t tests in **b, c**, **f**, and **g**. *, P<0.05; **, P<0.01; ***, P<0.001. For gel source data, see Supplementary Fig. 1. All mice in **d–i** were C57BL/6 *ATTAC.* +AP, AP-treated mice, –AP, vehicle-treated mice.

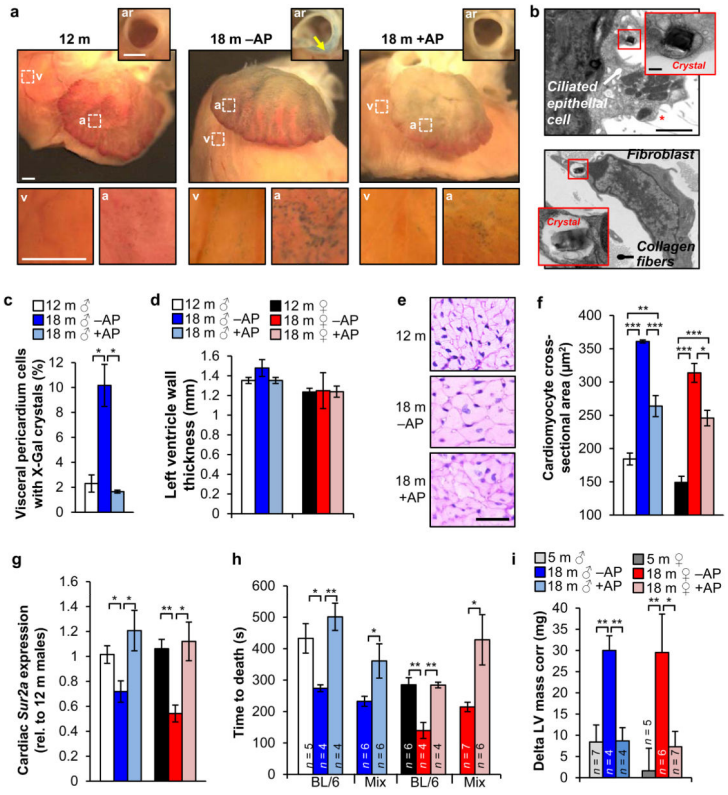

Figure 5. Senescent cells promote age-related cardiomyocyte hypertrophy and loss of cardiac stress tolerance

a, SA-β-Gal stained hearts. Insets show aortic roots (ar) from a transverse plane (arrow marks the aortic root wall) or closups of the ventricular (v) and arterial (a) boxed areas. **b**, Electron micrographs of X-Gal positive cells in the pericardium (red asterisk marks cilia). Insets show closeups of X-Gal crystals. **c**, Quantification of cells with X-Gal crystals in the visceral pedicardium (n = 4 mice per treatment). **d**, Measurements of left ventricle wall thickness (n = 4 mice per group). **e**, Representative cardiomyocyte cross-sectional images (n = 4 mice per group). **f**, Quantification of (**e**). **g**, Analysis of *Sur2a* expression in hearts by qRT-PCR (n = 4 mice per group). **h**, Cardiac stress resistance determined by measuring the time to death after injection of a lethal dose of isoproterenol. **i**, Change in left ventricular (LV) mass in response to sublethal doses of isoproterenol (10 mg.kg^{-1}) after ten doses administered over 5 days. Scale bars: 1 mm in **a**; 2 μm (main panel) and 200 nm (inset) in **b**. Legends in **f–h** are as in **d**. Error bars indicate s.e.m. Statistical significance was determined by unpaired two-tailed t test in **c, d** and **f–i**. *, P<0.05; **, P<0.01; ***, P<0.001. All mice, except for **h,** were C57BL/6 *ATTAC*. +AP, AP-treated mice, –AP, vehicle-treated mice.